Journal of Alloys and Compounds 509 (2011) 5571–5580

Contents lists available at ScienceDirect

Journal of Alloys and Compounds

journal homepage: www.elsevier.com/locate/jallcom

Twinning, dynamic recovery and recrystallization in the hot rolling process of twin-roll cast AZ31B alloy

Zhen Zhang[a,b,*], Ming-pu Wang[a], Zhou Li[a], Nian Jiang[a], Shimeng Hao[a], Jing Gong[a], Hailong Hu[a]

[a] School of Materials Science and Engineering, Central South University, Changsha, 410083,China
[b] Centre for Material and Fibre Innovation, ITRI, Deakin University, Geelong, VIC 3216, Australia

ARTICLE INFO

Article history:
Received 13 December 2010
Received in revised form 6 February 2011
Accepted 7 February 2011
Available online 12 February 2011

Keywords:
Magnesium alloy
Thermo-mechanical processing
Twinning
Recrystallization
Transmission electron microscopy

ABSTRACT

Hot-rolling experiments with a reduction from 10% to 60% in single pass were conducted on AZ31B twin-roll cast sheets. Optical microscope (OM), electron backscattered diffraction (EBSD) tests and transmission electron microscope (TEM) were used to investigate twinning and DRV/DRX behaviors at different stage in the hot-rolling process. Two types of twinning occurred in the initial stage of hot-rolling process. DRV and discontinuous recrystallization dominated at moderate strain while continuous DRX took place homogeneously throughout original grains at the largest strains.

1. Introduction

In recent years, magnesium alloys have attracted increasing interests in the field of automotive, aerospace due to their excellent properties such as low densities, heat dissipation, electro-magnetic shielding, etc.

However, magnesium alloys show poor plasticity due to their limited slip systems in the less symmetric hcp structure particularly at room temperature [1–3]. The most preferred slip system $(0002)\langle 11\bar{2}0\rangle$ could only provide two independent slip directions, with no capability of accommodating strain along C-axes. Twinning would thus readily participate as an effective deformation mechanism. Two types of twins, $\{10\bar{1}2\}$ tension twins and $\{10\bar{1}1\}$ compression twins, have been frequently reported in magnesium alloys [4–8], but most studies were concerned with twinning orientation at small strains or low temperature [9–15]. How twinning behaviors and its influence on microstructure evolution at large strain is still unclear today. Also as we know, for the successful application of wrought magnesium alloy sheet products, thermo-mechanical processing technology, such as hot/warm rolling, is usually adopted to obtain excellent formability and mechanical properties. Two typical characteristics in warm/thermal processing of magnesium alloys are dynamic recovery (DRV) and recrystallization (DRX) [16–20]. They were invariably represented as an occurrence of peak stress or steady flow stage in stress–strain curves, which were frequently observed in isothermal compression and tensile test of magnesium alloys [21–23]. Although a number of DRX mechanisms, such as twin dynamic recrystallization (TDRX) [24–26], low temperature DRX (LTDRX) [27], continuous dynamic recrystallization (CDRX) [28], discontinuous dynamic recrystallization (DDRX) [23], rotational dynamic recrysallization (RRX) [29], etc, have been introduced in magnesium alloys, their kinetic processes were rarely discussed. Dynamic recovery is generally considered to take place in materials with high stacking fault energy (SFE) meanwhile dynamic recrystallization is thought to be dominative in materials with low SFE [30]. However, it is really difficult to strictly distinguish these two processes and actually they would have mutual effect on each other, as suggested by Al-Samman and Gottstein in [31]. The present work aimed to demonstrate the kinetic processes of DRV/DRX and their relation, as well as to give a brief description on twinning behaviors and their influence on microstructure evolution in thermo-mechanical process.

In the present study, single pass hot-rolling experiments with a thickness reduction from 10% to 60% were performed on AZ31B twin-roll cast (TRC) sheet. OM, EBSD tests and TEM were used to investigate twinning and DRV/DRX behaviors at different stages.

* Corresponding author at: School of Materials Science and Engineering, Central South University, Changsha, 410083, China. Tel.: +86 13874963491; fax: +86 731 88876692.
E-mail address: turkeyzz1984@gmail.com (Z. Zhang).

0925-8388/$ – see front matter.
doi:10.1016/j.jallcom.2011.02.040

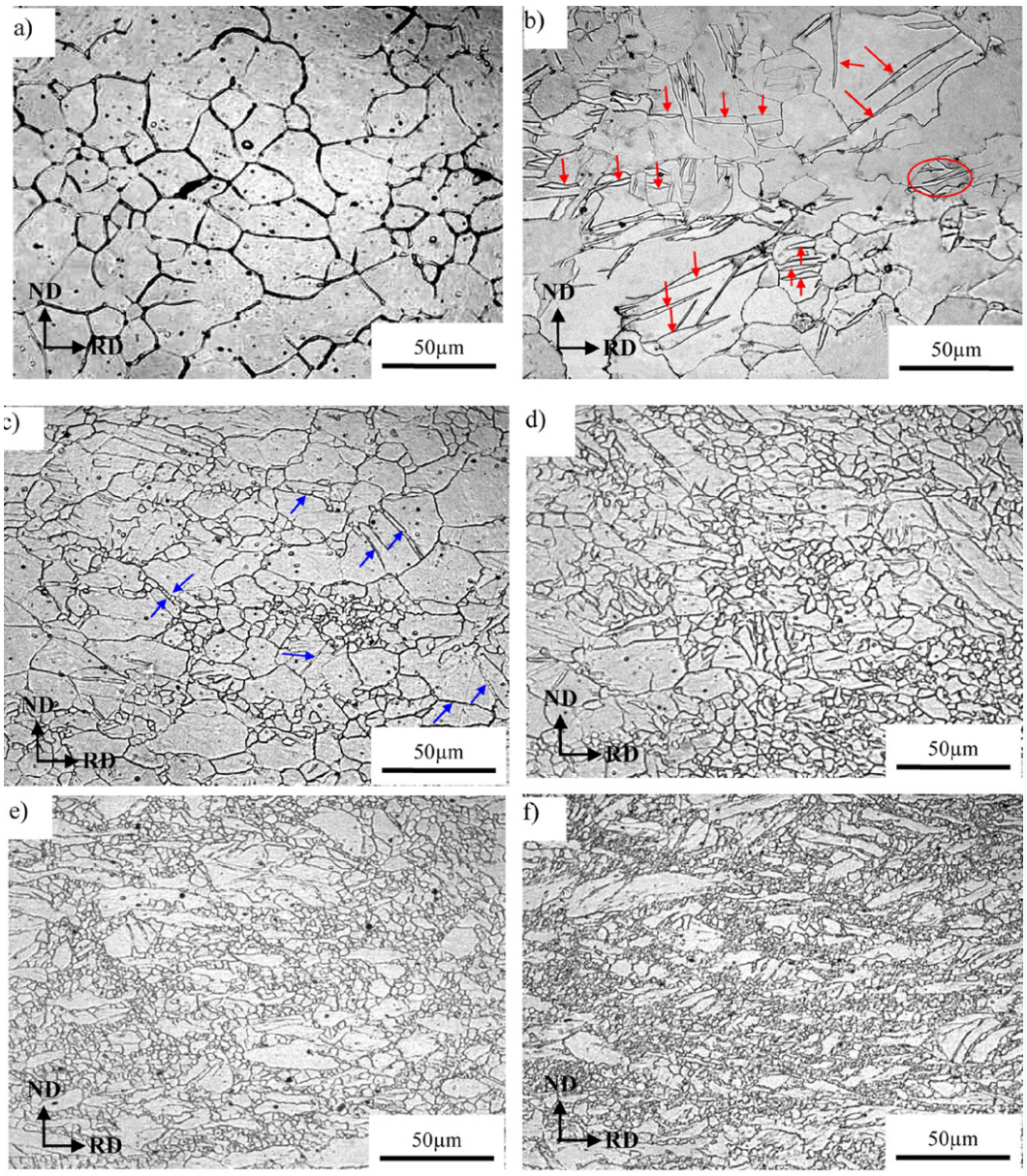

Fig. 1. Optical micrograph showing the microstructure of (a) homogenized TRC sheet and hot-rolled sheet with a reduction of (b) 10%, (c) 20%, (d) 30%, (e) 50% and (f) 60% respectively.

2. Experimental

The material used in this study was AZ31B sheets fabricated by twin-roll cast (TRC) method. The nominal composition is 3 wt% Al, 1 wt% Zn and balance Mg. The TRC sheets were initially homogenization annealed at 430 °C for 2 h. Samples with dimensions of 3 cm × 10 cm × 6.4 mm were cut from the homogenized sheet and subsequently hot-rolled in single pass with a thickness reduction from 10% to 60% at 375 °C. Larger rolling reduction would cause extensive side crack and 375 °C was chosen as working temperature in order to avoid the precipitation of β-phase ($Mg_{17}Al_{12}$) [19,31,32].

Metallographic observation was conducted on the RD-ND plane using Leica EC3 optical microscopy. The samples were mechanical polished and etched using a solution of picric–acetic. EBSD measurements were carried out for 10% and 20% hot-rolled samples on the RD-ND plane using FEI Sirion200 FEG SEM operated at 15 kV. Sample preparation for EBSD tests consisted of grinding on SiC papers with grid sizes of 600, 800, 1200, followed by mechanical polishing and final electrolytic polishing with commercial AC-2 electrolyte conducted under 35.4 V at −30 °C. Statistic orientation analyses were processed using OIM TSL software provided by EDAX. TEM observation was carried out for 20%, 30%, 60% hot-rolled samples on FEI Tecnai G^2 operated at 200 kV. The specimens were firstly sectioned parallel to the RD-ND plane, grounded to 100 μm, then punched into Ø 3 mm discs and finally double-jet electrolytically polished to make a thin area with commercial AC-2 electrolyte under the same condition as EBSD samples preparation.

3. Results

3.1. Optical microstructure observation

Fig. 1 shows the microstructure evolution of AZ31B TRC sheets during hot-rolling process. The original microstructure of homogenized TRC sheets was equiaxed grains with a mean size of about 25 μm. After 10% rolling reduction, extensive lenticular twins formed in original grains, as indicated by arrows in Fig. 1(b). No evident recrystallization was found within these twins or matrices. Compared with those lenticular twins found in 10% rolled sheets, thin twins with totally different morphology were produced in 20% rolling process, as indicated by arrows in Fig. 1(c). Moreover, some fine recrystallized grains appeared at original grain boundaries and within twinned regions. As rolling reduction increased to 30%, the microstructure got inhomogeneous, and grain fragmentation became the most typical morphology in the 50% and 60% hot-rolled samples. In the present work, rolling reduction could reach as high as 60% without evident crack. So a reduction between

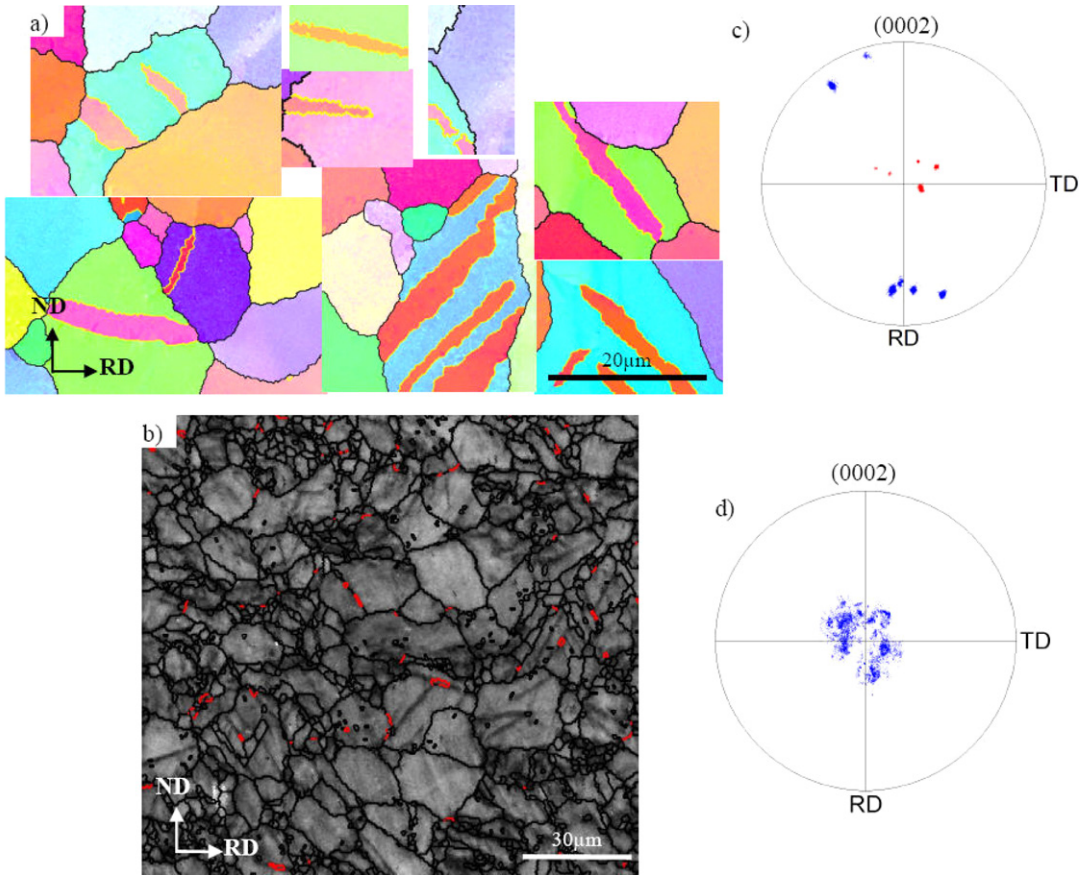

Fig. 2. (a) OIM maps of 10% and (b) an IQ map of 20% hot-rolled samples, the orientation of grains which have twinned were presented in (0 0 0 2) discrete pole figures for (c) 10% (matrix in blue, twinned region in red) and (d) 20% samples. (For interpretation of the references to color in this figure legend, the reader is referred to the web version of the article.)

50% and 60% would be a good choice for industrial rolling process of this TRC alloy, considering the production efficiency.

3.2. EBSD measurement

As described above, two kinds of twins were found at initial strain stage of rolling process. To investigate these twinning characteristics, EBSD measurements were conducted for the 10% and 20% hot-rolled samples. Fig. 2(a) shows the OIM maps of 10% rolled samples. Boundaries with misorientation of $87 \pm 2^\circ$ along $\langle 1\,1\,\bar{2}\,0\rangle$, which were expected for $\{1\,0\,\bar{1}\,2\}$ twins, were highlighted in yellow. It could be seen that all the lenticular twins produced in 10% rolling process belonged to $\{1\,0\,\bar{1}\,2\}$ type. Fig. 2(b) shows an IQ map of a 20% hot-rolled sample, which bases on the contrast of Kikuchi bands. Thin twins were found prevalent across the image and recrystallization has already occurred in some of these twins. These were in accord with the results obtained from metallographic observation. Probably due to the high strain location inside these thin twins, contrast of Kikuchi bands was usually poor in these regions. So only a few fragments of boundaries with misorientation of $56 \pm 2^\circ$, which was expected for $\{1\,0\,\bar{1}\,1\}$ twins, were found at some twin boundaries.

In addition, the matrix orientations of grains, which contained twins inside were represented in (0 0 0 2) discrete pole figures (DPF), as shown in Fig. 2(c) and (d). It could be revealed that all the thick lenticular $\{1\,0\,\bar{1}\,2\}$ twins in 10% rolled samples were produced in grains with their C-axes located close to the edge of the DPF while all the thin twins formed in grains with their C-axes close to the center of the DPF.

3.3. TEM observation

3.3.1. 20% hot-rolled samples

The most distinctive feature in 20% rolled samples was the thin twins, which tended to be preferred sites for local recrystallization nucleation. However, the contrast of Kikuchi bands within these twinned regions was usually too poor to index in EBSD tests as described in Section 3.2. TEM analyses were thus conducted.

The selected area electron diffraction (SAED) pattern taken from the twinned area in Fig. 3(a) indicated a $\{1\,0\,\bar{1}\,1\}$ twinning type, as shown in Fig. 3(b). In addition, the dislocations coincided well with the trace of $(1\,0\,\bar{1}\,0)$ plane both in the twin and matrix. As we know, only three types of dislocations $\vec{a}$, $\vec{c}$, $\vec{a}+\vec{c}$, have been reported in magnesium alloys. Double-beam condition was set up to measure the Burges vectors of these dislocations in matrix. These dislocations were thus expected to have a non-basal component since they were in contrast when $\vec{g} = (0\,0\,0\,2)$ in Fig. 3(c), while keeping in contrast when $\vec{g} = (1\,0\,\bar{1}\,0)$ in Fig. 3(d), excluded their possibility of being $\vec{c}$ dislocations. Furthermore, the extinction of these dislocations when $\vec{g} = (1\,0\,\bar{1}\,1)$, as shown in Fig. 3(e), would finally confirm that these dislocations were lying on $(1\,0\,\bar{1}\,0)$ plane with a Burges vector of $\vec{a}+\vec{c}$. As could be seen clearly in Fig. 3(f) and (g), these dislocations in the parent grain usually accumulated at these twin boundaries and some dislocation substructures were formed at boundaries or inside the twins, where dynamic recrystallization tended to nucleate.

3.3.2. 30% hot-rolled samples

Fig. 4(a) shows a panorama of a grain of a size about 25 μm in a 30% rolled sample. A bundle of slip bands traversed the grain,

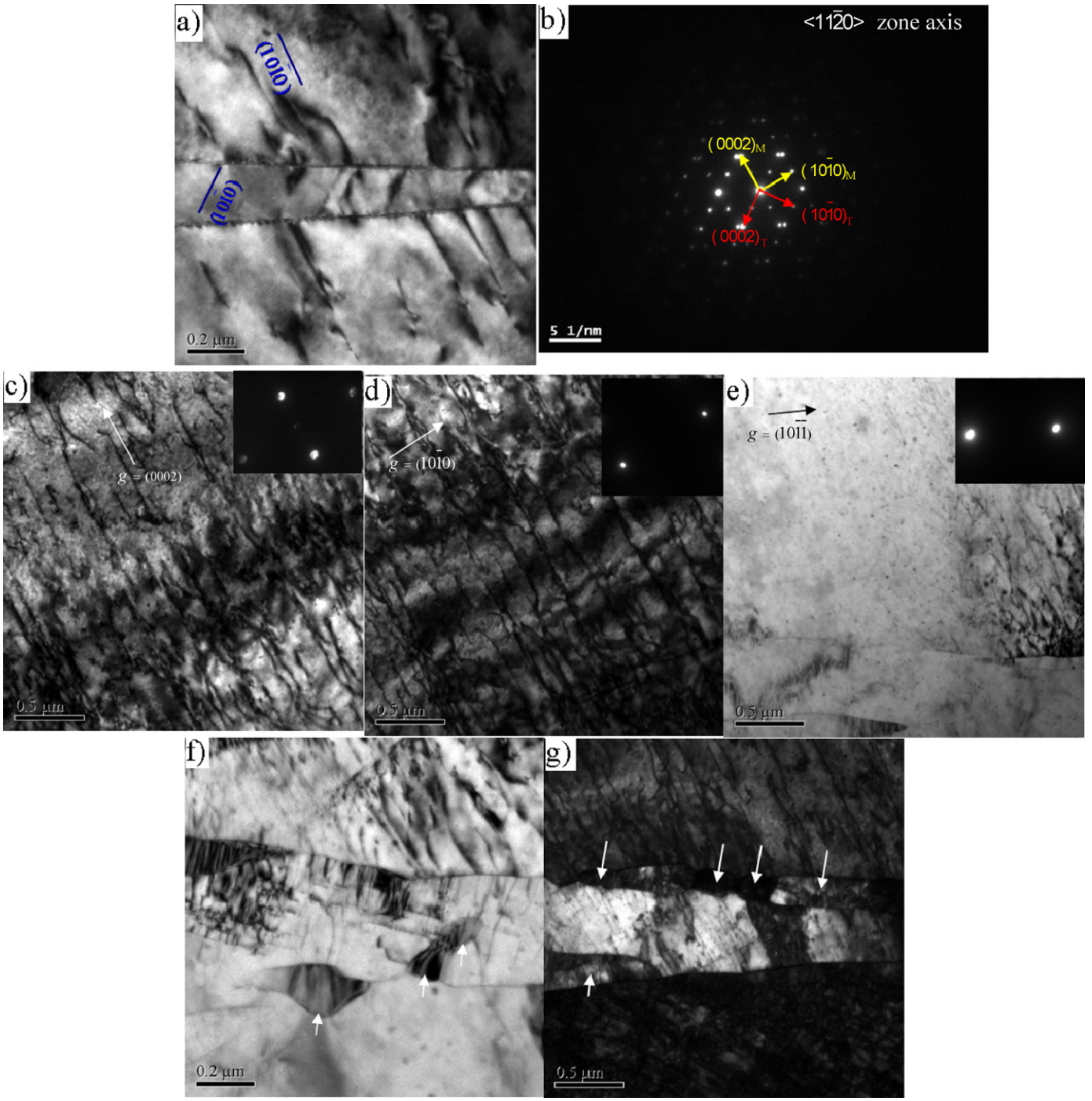

Fig. 3. (a) A thin twin in 20% hot-rolled sample and (b) its SAED pattern, dislocations in the parent grain were in contrast when with (c) g = (0 0 0 2), (d) g = {1 0 $\bar{1}$ 0}, and lost contrast when (e) g = {1 0 $\bar{1}$ 1}, simultaneously DRX grains began to initiate at the twinned region (f) and (g).

dividing it into two parts. These band boundaries were found to consist of regular arrays of dislocation lying on the (0 0 0 2) plane. It was reasonable to think that the directions of these dislocations were nearly parallel to ⟨1 1 $\bar{2}$ 0⟩ since they looked rather short in the TEM image taken along ⟨1 1 $\bar{2}$ 0⟩ zone axis. As the most easily activated slip system in magnesium is (0 0 0 2) ⟨11$\bar{2}$0⟩, the high density of dislocations on these slip bands suggested that extensive basal slip has proceeded on certain (0 0 0 2) planes and finally congregated to form such bands. As there is only one equivalent (0 0 0 2) plane in the less symmetrical hcp structure, slip bands formed in magnesium alloys were supposed to walk along only one direction within individual grains unlike the rhombic slip bands formed in fcc metals [33]. Simultaneously, SAED pattern taken across a slip band revealed a small misorientation of about 3°, as shown in Fig. 4(b) and (c). It was thought that small orientation variation has been already generated at this strain within original grains via the formation of slip bands.

At the same time, DRX began to initiate along original grain boundaries, indicated by arrows in Fig. 4(a). The region of the blue rectangle at lower right corner was magnified for details as shown in Fig. 5(a) and (b). It showed that dislocations began to accumulate at the triple joint of grain boundary and some of them have been rearranged into a dislocation wall. Nucleation of the recrystallized grain, denoted as 'A' in Fig. 5(b), was accompanied by local migra-

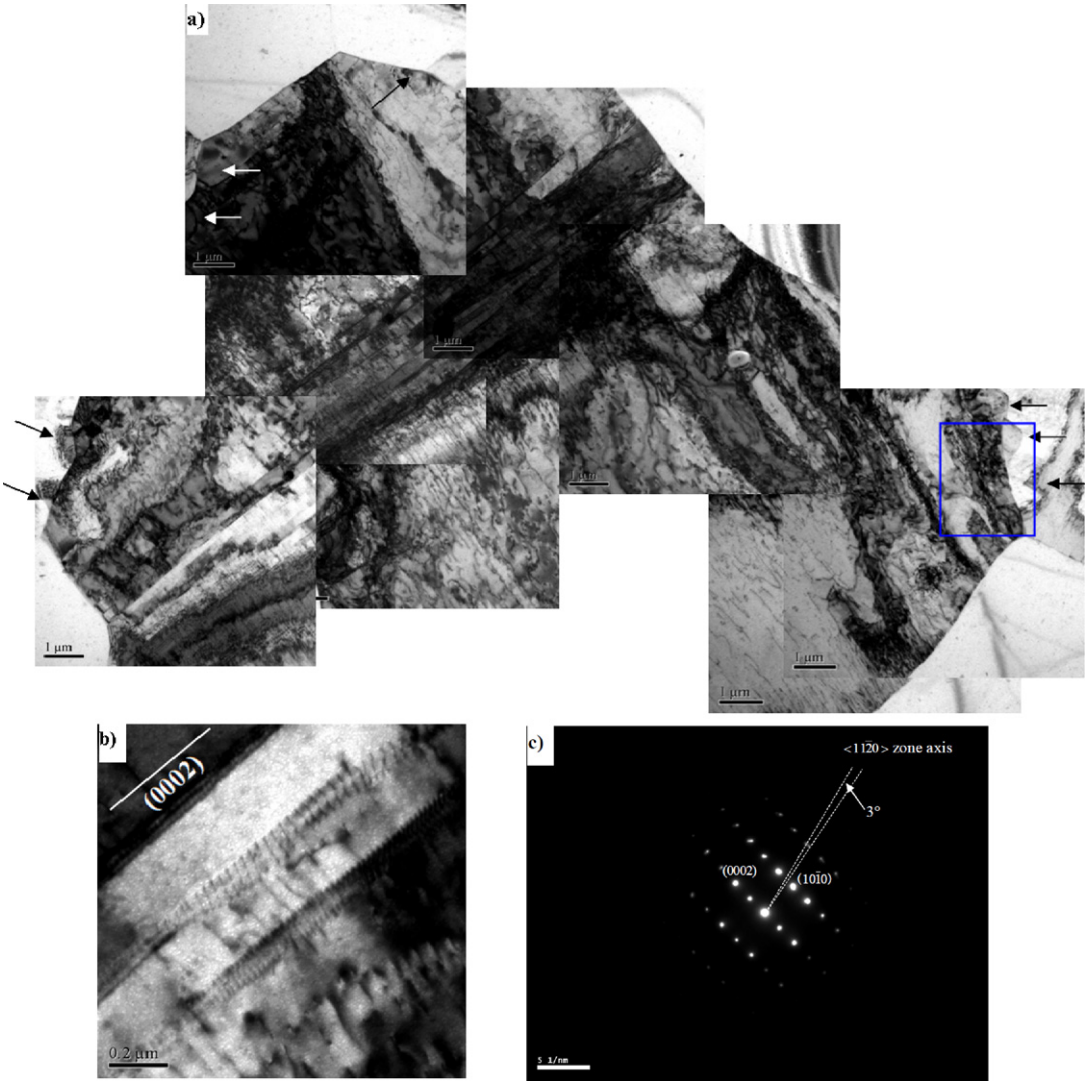

Fig. 4. (a) A panorama for a grain of a size about 25 μm in a 30% rolled sample and (c) SAED pattern taken across a slip band in (b).

tion of original grain boundary, behind which dislocations tangled and had a tendency to cut off the expanding protrusion from the parent grain. No dislocation could be found in the swept volume of original grain boundary, however. It was supposed to be the characteristic of typical discontinuous recrystallization, which has been regularly found in a wide variety of metals particularly after low strains [30] (also called Strain Induced Grain Boundary Migration (SIBM) in some literatures). Some serrated boundaries caused by grain boundary migration have also been found elsewhere in the same sample as indicated by arrows in Fig. 5(c).

Fig. 6(a) shows a subgrain formed at the boundary of an original grain. SAED pattern taken at this region indicated a single crystal characteristic. Grain boundary migration was not involved and dislocations were rarely found in the subgrain or parent grain. Such substructure formation was expected to be a recovery dominated process since the boundary was made up of regular arrays of dislocations, as shown in Fig. 6(b) and (d). AB segment of the boundary in Fig. 6(b) coincided well with the $(1\,0\,\bar{1}\,1)$ plane, and these dislocation directions were thought to be close to $\langle 1\,1\,\bar{2}\,0\rangle$, as they looked rather short in the TEM image along $\langle 1\,1\,\bar{2}\,0\rangle$ zone axis, which lies on the basal plane. Dislocations on BC segment were lying exactly on $(0\,0\,0\,2)$ plane while the dislocations on DE segment were presented as almost dots shape from $\langle 1\,1\,\bar{2}\,0\rangle$ zone axis as shown in Fig. 6(c) and (d). It was supposed that all these dislocations constructing subboundaries were lying exactly on or close to the basal plane, which may imply that basal slip would play an important role in such DRV dominated process.

At the same time, a dislocation wall, which has a rather irregular shape formed at original grain boundary. SAED pattern taken along $[1\,0\,\bar{1}\,0]$ zone axis defined the trace of $(0\,0\,0\,2)$ and $(1\,1\,\bar{2}\,0)$ plane in the image, which is shown in Fig. 7(a). Although showing different length in the image, the dislocations constructing the wall all invariably coincided with the basal trace. It simply stated that these dislocations were lying on the basal plane and the closer they inclined to $[1\,0\,\bar{1}\,0]$, the shorter they projected to the image. AB segment of this wall was parallel to $(1\,1\,\bar{2}\,2)$ trace and the dislocations lying on this segment looked rather short, which may imply that they were close to the $[1\,0\,\bar{1}\,0]$ zone axis. However, other parts of this wall showed irregular arranging plane and revealed a gradually rotation of dislocation direction towards $\langle 1\,1\,\bar{2}\,0\rangle$ as they spanned the grain, approaching the other side of this grain. A reasonable scheme of such dislocation arrangement is presented in Fig. 7(c). Double-beam condition was performed to measure the Burges vector of these dislocations. All the dislocations lost their contrast when the diffraction vector $\vec{g}$ was $(0\,0\,0\,2)$, as shown in Fig. 7(b), which would completely confirm that all these dislocations owned a Burges vector of $\vec{a}$.

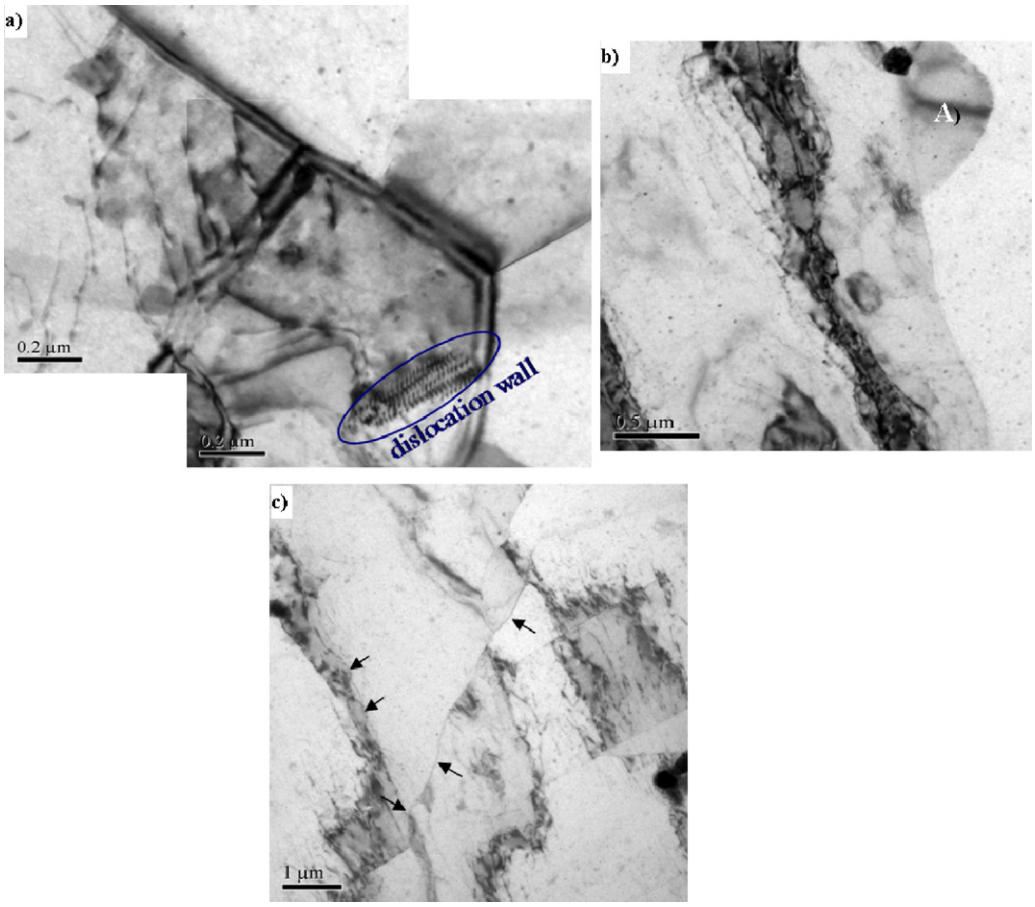

Fig. 5. (a) A substructure formed at triple joint of grain boundaries, (b) a recrystallized grain formed via migration of original grain boundary, (c) serrated grain boundary caused by migration of grain boundary found elsewhere in 20% rolled sample.

Also it could be seen that non-basal dislocations have been activated and started cross-slipping near the grain boundary, as indicated by arrows in Fig. 7(a), and the major parts of these non-basal dislocations were lying on the $(1\,1\,\bar{2}\,0)$ plane. A substructure was found to initiate at the grain boundary where non-basal slip was extensively activated as shown in Fig. 7(d), which could be thought as a prerequisite stage in the formation of a substructure.

3.3.3. 60% rolled samples

Fig. 8(a) shows the substructures within a grain in a 60% rolled sample. Dislocation slip was more homogeneously activated across the whole grain, producing widespread cellular structures inside the original grain, indicated by white arrows. In addition, a number of dislocation walls were found near the original grain boundary, marked with yellow arrows in the image. SAED pattern taken across the whole grain revealed split-ups of diffraction spots, as shown in Fig. 8(b). It thus manifested some orientation spread across the grain, which may be attributed to the formation of cellular structures. Furthermore, dynamic recrystallization began to nucleate on the basis of previously formed cellular structures in the vicinity of original grain boundary, as shown in Fig. 8(c).

4. Discussion

4.1. Microstructure evolution in hot-rolling process

Similar to the results obtained in uniaxial compression experiments, twining also played an important role in the initial strain stage of rolling process [31]. After rolling with 10% reduction, $\{1\,0\,\bar{1}\,2\}$ twinning took place in grains whose C-axes were nearly perpendicular to ND, and the twinned region changed to new orientations with C-axes more aligned with ND, as indicated in Fig. 2(c). In addition, $\{10\bar{1}2\}$ twins had a tendency to consume the entire volume of parent grains probably due to the high mobility of $\{1\,0\,\bar{1}\,2\}$ twin boundary [5] and the lowest shear among all possible twinning systems in magnesium alloys [35]. There would be little doubt that these were important reasons for the universal observation of this twinning mode [5,8,10,11,29]. It simply indicates that after initial 10% rolling reduction $\{1\,0\,\bar{1}\,2\}$ twinning occurred in such a way that made most grains to 'basal orientations' [34]. After completely orientation change via $\{1\,0\,\bar{1}\,2\}$ twinning, thin $\{1\,0\,\bar{1}\,1\}$ twins were produced in these grains with 'basal orientation', as observed in 20% rolled samples. Recrystallization was apt to nucleate at these $\{1\,0\,\bar{1}\,1\}$ twinned regions rather than in the thick $\{1\,0\,\bar{1}\,2\}$ twins. This twinning-related recrystallization will be discussed separately below. With the increase of rolling reduction, dislocations congregated on certain basal planes, producing simple slipping bands inside original grains. Consequently, orientation variation was generated across original grains, and recovery related substructures formed inhomogeneously at grain boundaries. Basal dislocation seemed to play a most important role in recovery process. At the same time, discontinuous recrystallization took place, accompanied by the migration of original grain boundaries, producing serrated grain boundaries. At even larger strains, dislocation slip occurred extensively and more homogeneously, and widespread cellular structures were formed across whole grain volume, which indicated the incubation of continuous dynamic recrystallization. Cellular structures may provide preferred sites for this recrystallizaiton nucleation.

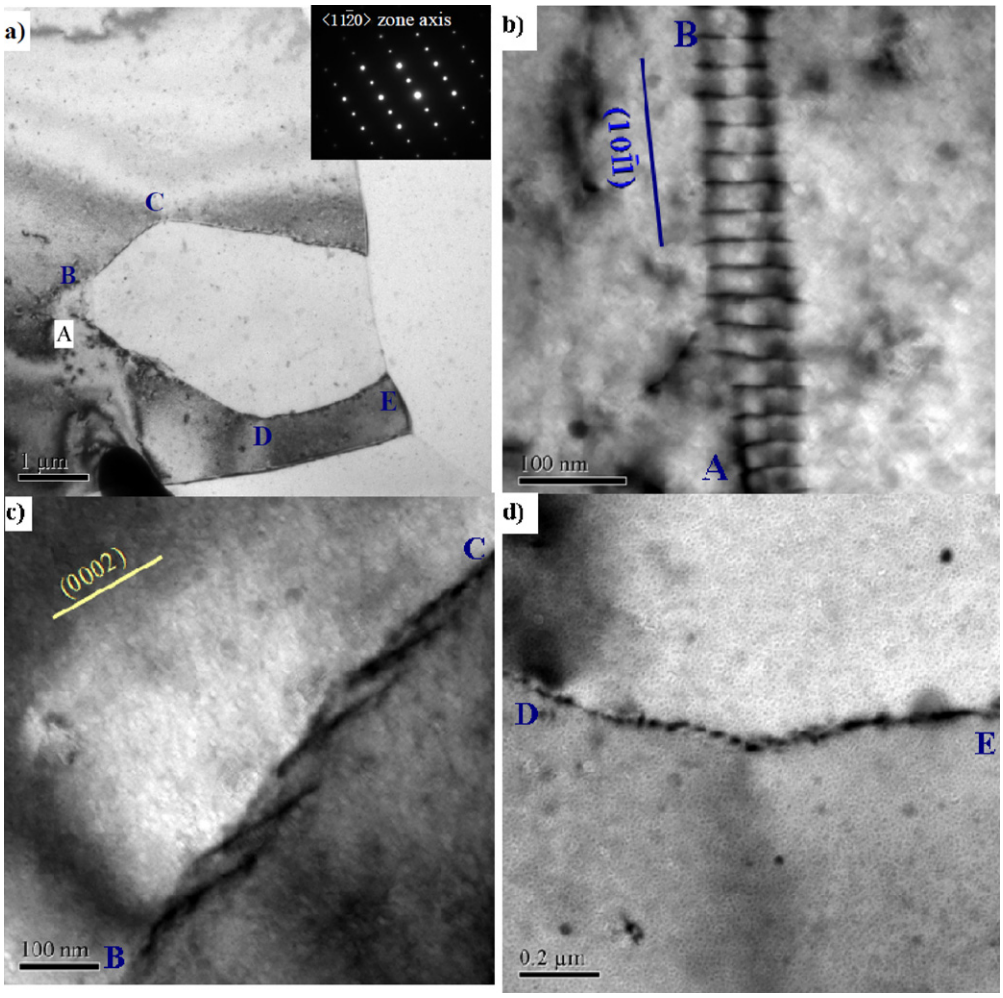

Fig. 6. A TEM image of (a) a subgrain formed adjacent to an original grain boundary and magnification of boundary segment of (b) AB, (c) BC and (d) DE.

4.2. Twinning and twinning-induced recrystallization

Two types of twins were produced in the rolling process, as described in Section 3.2. During the first 10% rolling reduction, $\{1\,0\,\bar{1}\,2\}$ twinning occurred in grains about 90° from basal orientation, as indicated in Fig. 2(c). These twins usually owned a stable misorientation 87° $\langle 1\,1\,\bar{2}\,0\rangle$ with matrix and had a tendency to consume whole grains. Unlike the $\{1\,0\,\bar{1}\,2\}$ twins produced in 10% rolling process, the $\{1\,0\,\bar{1}\,1\}$ twins in 20% rolled samples looked much thinner in optical microstructure and tended to be preferred sites for recrystallization nucleation. It has been frequently reported that lattice rotation always took place within thin compression twins in magnesium single crystals orientated with C-axes in compression [8,10,11]. Hartt and Reed-Hill [11] attributed this to kinking occurring by slip on $\{1\,0\,\bar{1}\,1\}\langle 11\bar{2}3\rangle$, which would have been activated under concentrated shear directed with the help of proximity of the twin boundaries to each other. This could be also expected in our experiment. As in the present study, thin $\{1\,0\,\bar{1}\,1\}$ twins were always initiating in grains with C-axes in compression, where $\vec{a}+\vec{c}$ slip system acquired much higher resolved stress. Non-basal slip thus occurred extensively in matrix and accumulated at twin boundaries, producing high stress concentration in these areas, as shown in Fig. 3. Simultaneously due to the minute width of these twins, the plastic compatibility stress of twin boundaries would readily influence the whole volume of such twins, non-basal slip could thus be easily activated and develop throughout the whole twinned region immediately. Abound dislocation slip occurring within twined region would act as kinetic process for substructure formation and provide preferred sites for DRX nucleation, as shown in Fig. 3(f) and (g).

4.3. Dynamic recovery and recrystallization

Dynamic recovery may readily take place at moderate strain, which was 30% in the present work, as so many dislocation walls and subgrains were observed. Similar results have been reported in the cross-rolling of AZ31 TRC sheet in [31]. This could be expected considering the high working temperature and the somewhat higher stack fault energy (SFE) of magnesium alloy compared with Au, Ag, Cu alloys [36,37]. Basal dislocations played an active role in constructing dislocation walls, rearranging along certain planes or irregularly inside original grains, as shown in Figs. 5–7. This is similar to the phenomenon observed in single crystals, which were deformed on a single slip system [30]. At the same time, three dimensional (3D) substructures were usually found near grain boundaries where non-basal slip was activated readily. As we know, basal slip could only provide two independent slip directions in hcp structure, much less than the ordinary slip system $(1\,1\,1)\langle 1\,1\,0\rangle$ in more symmetrical fcc metals. It is thus reasonable to think that the activation of non-basal slip meets the requirement for the formation of 3D substructures in magnesium alloys. And such non-basal slip was expected to occur in the neighborhood of grain boundaries where stress concentration arose due to continuous slip of basal dislocations and their pile-

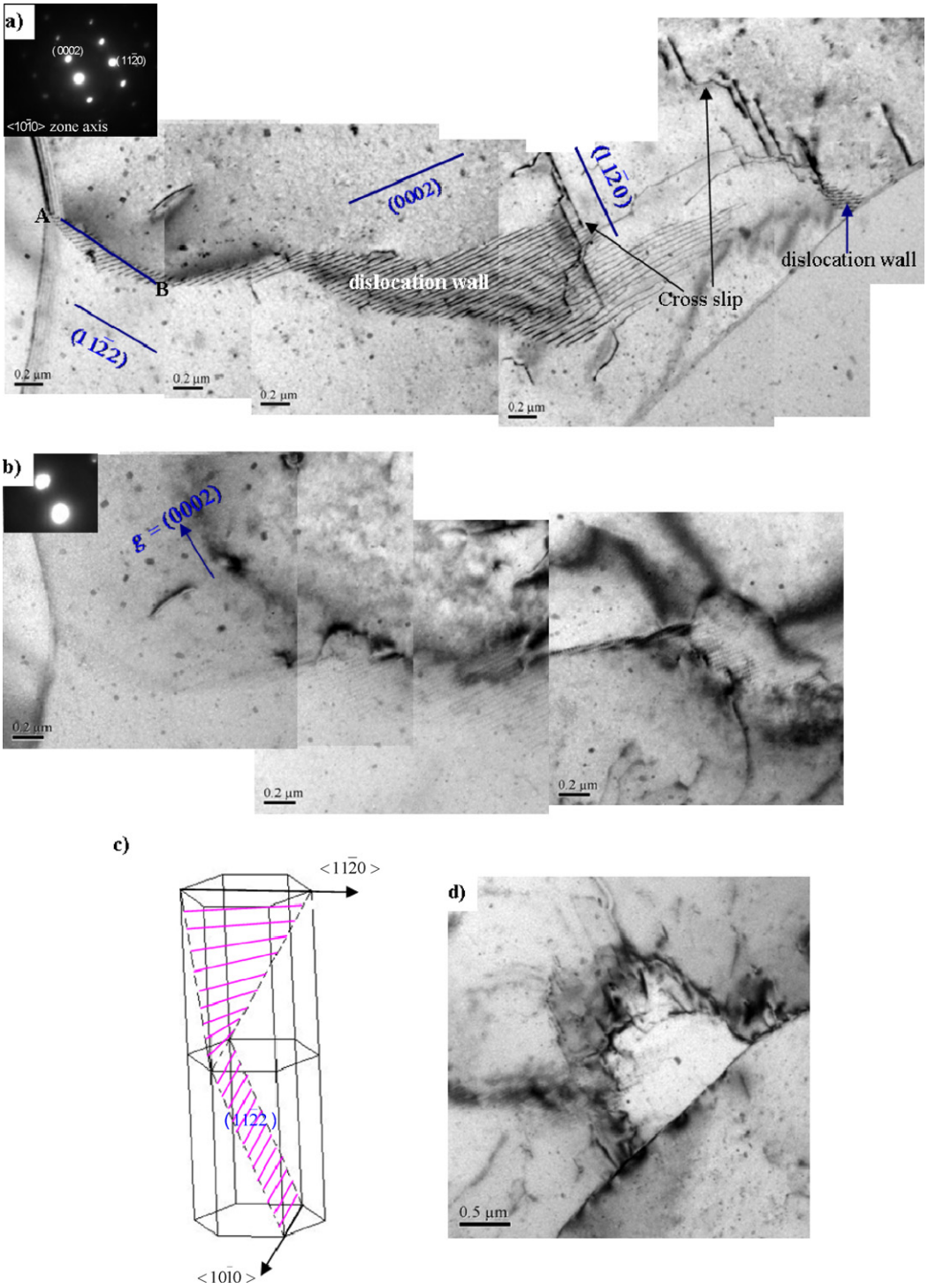

Fig. 7. (a) TEM image of a dislocation wall formed across an original grain, (b) the constructing dislocations loose their contrast when g = (0 0 0 2), (c) a scheme of dislocation arrangement on this dislocation wall (d) a substructure initiated at the grain boundary where non-basal slip was activated.

ups in these areas. Simultaneously, the plastic compatibility stress of grain boundaries may also contribute to the easy activation of non-basal slip in these areas [38]. Furthermore, some serrated grain boundaries and concomitant subgrains adjacent to them were also observed at moderate strain, seen in Fig. 5, which indicated the process of grain migration—the characteristic of discontinuous recrystallization. Valiev et al. [39] explained that serrated boundaries formed when the proceeding dislocations entering grain boundaries exceeded their absorption capacity or when the process of lattice dislocation absorption requires an incubation time. These excessive dislocations then piled up and subsequently generated a local stress concentration at grain boundaries, resulting in their migration. The pile-up dislocations would finally cut off the new formed grains from matrix behind the swept volume.

As rolling reduction increased to 60%, non-basal slip occurred more homogeneously throughout original grains, where cellular structures became prevalent over the whole volume, as shown in Fig. 8. Consequently, continuous recrystallization began to nucleate on the basis of 3D substructures in the vicinity of grain boundaries. With the development of deformation, recrystallization expanded

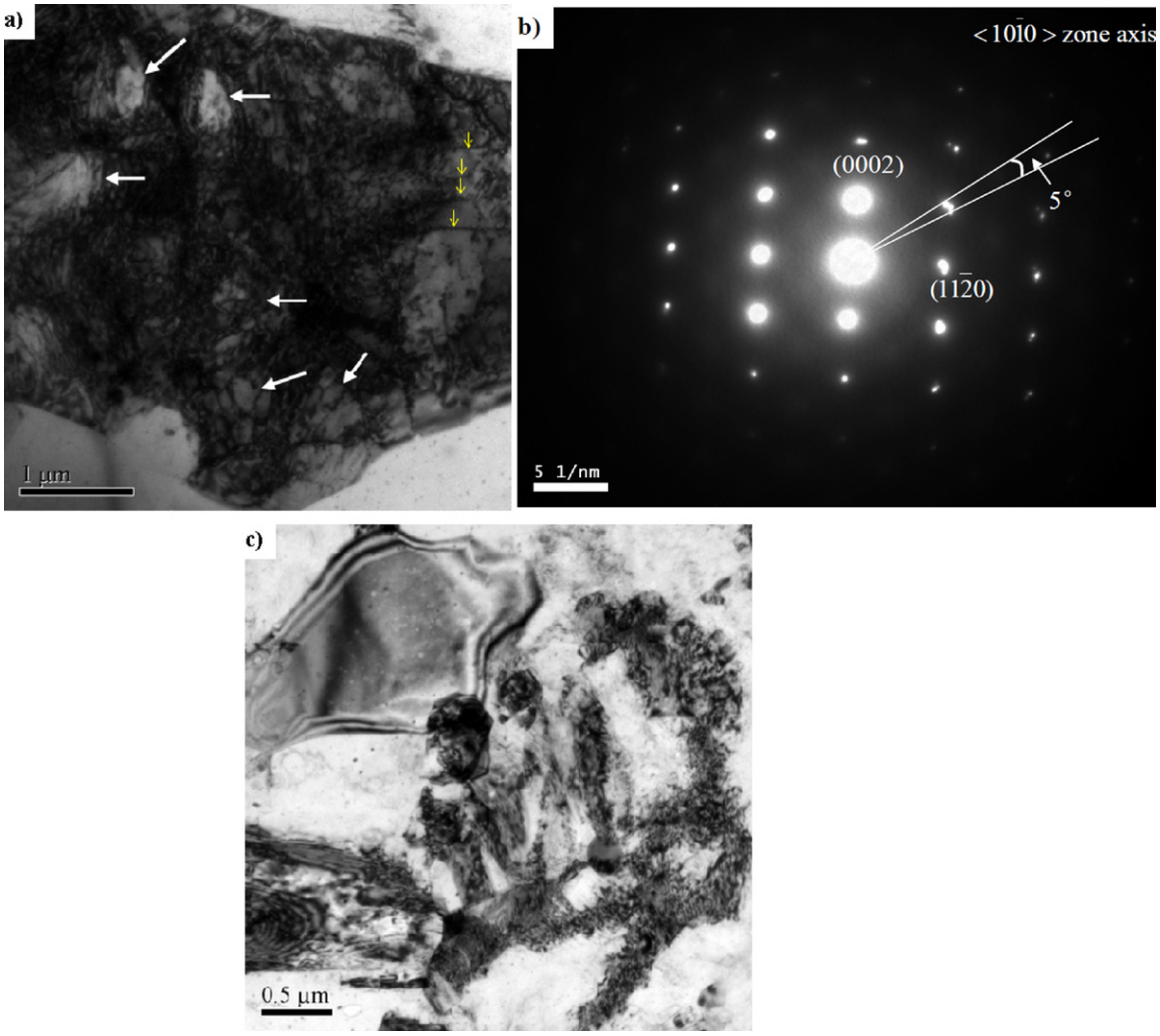

Fig. 8. (a) Cellular structures formed in an original grain after 60% rolling process and (b) SAED pattern taken from this region, (c) dynamic recrystallized grains nucleated near the previous formed cellular structures.

to grain interior gradually. It was generally considered as a recovery related process, which induced gradual increase in the misorientation of substructure and conversion of low-angle grain boundaries into high-angle boundaries. Previous studies on the DRX of aluminum alloys emphasized the importance of stable particles such Al_3Zr and Al_3Sc in stabilizing the substructure during continuous dynamic recrystallizaiton [40,41]. However, it was not the case for magnesium alloys, as Tan and Tan [17] found in uniaxial compression of AZ31B alloys. They attributed this to the lack of easily activated slip system and the high rate of grain boundary migration in magnesium alloys. In our present study, the formation of 3D substructure was frequently found to be accompanied by non-basal dislocations, which usually showed features of cross-slipping. It was probably that the jog segments of these dislocations lying on intermediate plane of cross-slipping were more sessile than the major segments. They would thus play a key role in stabilizing the substructures, which may provide a microstructure foundation for subsequent recrystallization nucleation.

5. Conclusions

Twinning played the most important role in the initial stage of hot-rolling process, which is less than 20% reduction in the present work. $\{1\,0\,\bar{1}\,2\}$ twins formed in grains whose C-axes were nearly perpendicular to ND and this twinning occurred in such a way that made whole matrix close to 'basal orientation'. Thin $\{1\,0\,\bar{1}\,1\}$ twins were produced in grains close to 'basal orientation' and became most preferred sites for recrystallization.

DRV and discontinuous recrystallization dominated in the deformation when the reduction reached 30%. Basal slip played a key role in DRV process while the activation of non-basal slip is an essential step in forming 3D substructure, which would be potential structure basis for DRX nucleation.

Non-basal slip was homogeneously activated at even larger strains of 60%, producing widespread cellular structures throughout the whole volumes of original grains. Consequently continuous DRX readily take place on the basis of these substructures.

Acknowledgement

The authors acknowledge financial support from Program 2004BA311A11-1 under the Ministry of Science and Technology of the PRC.

References

[1] G.R. Ebrahimi, A.R. Maldar, R. Ebrahimi, A. Davoodi, J. Alloys Compd. 509 (2011) 2703–2708.
[2] Sangbong Yi, Heinz-Günter Brokmeier, Dietmar Letzig, J. Alloys Compd. 506 (2010) 364–371.
[3] Horng-yu Wu, Wei-chien Hsu, J. Alloys Compd. 493 (2010) 590–594.

[4] M.R. Barnett, Mater. Sci. Eng. A 464 (2007) 1–7.
[5] M.R. Barnett, Mater. Sci. Eng. A 464 (2007) 8–16.
[6] S. Jiang, T. Liu, L. Lu, W. Zenga, Z. Wang, Scripta Mater. 62 (2010) 556–559.
[7] L. Guan, G. Tang, Y. Jiang, P.K. Chu, J. Alloys Compd. 487 (2009) 309–313.
[8] E.W. Kelley, W.F. Hosford, Trans. Metall. Soc. AIME 242 (1968) 654–660.
[9] B. Song, G. Huang, H.C. Li, L. Zhang, G.J. Huang, F.S. Pan, J. Alloys Compd. 489 (2010) 475–481.
[10] E.W. Kelley, W.F. Hosford, Trans. Metall. Soc. AIME 242 (1968) 5–13.
[11] W.H. Hartt, R.E. Reedhill, Trans. Metall. Soc. AIME 242 (1968) 1127–1133.
[12] M.R. Barnett, C.H.J. Davies, X. Ma, Scripta Mater. 52 (2005) 627–632.
[13] S.M. Fatemi-Varzaneh, A. Zarei-Hanzaki, M. Haghshenas, J. Alloys Compd. 475 (2009) 126–130.
[14] H.A. Patel, D.L. Chen, S.D. Bhole, K. Sadayappan, J. Alloys Compd. 496 (2010) 140–148.
[15] T.S. Srivatsan, S. Vasudevan, M. Petraroli, J. Alloys Compd. 461 (2008) 154–159.
[16] J.A. del Valle, M.T. Pérez-Prado, O.A. Ruano, Mater. Sci. Eng. A 410–411 (2005) 353–357.
[17] J.C. Tan, M.J. Tan, Mater. Sci. Eng. A 339 (2003) 124–132.
[18] M.T. Pérez-Prado, J.A. del Valle, J.M. Contreras, O.A. Ruano, Scripta Mater. 50 (2004) 661–665.
[19] J.A. del Valle, M.T. Pérez-Prado, O.A. Ruano, Mater. Sci. Eng. A 355 (2003) 68–78.
[20] Qing Miao, Lianxi Hu, Xin Wang, Erde Wang, J. Alloys Compd. 493 (2010) 87–90.
[21] S.M. Fatemi-Varzaneh, A. Zarei-Hanzaki, H. Beladi, Mater. Sci. Eng. A 456 (2007) 52–57.
[22] L. Helis, K. Okayasu, H. Fukutomi, Mater. Sci. Eng. A 430 (2006) 98–103.
[23] A. Galiyev, R. Kaibyshev, G. Gottstein, Acta Mater. 49 (2001) 1199–1207.
[24] M.M. Myshlyaev, H.J. Mcqueen, A. Mwembela, E. Konopleva, Mater. Sci. Eng. A 337 (2002) 121–133.
[25] C.M. Liu, Z.J. Liu, X.R. Zhu, Chin. J. Nonferrous Met. 16 (2006) 1–12.
[26] T.A. Samman, G. Gottstein, Mater. Sci. Eng. A 490 (2008) 411–420.
[27] Z.Y. Liu, S. Bai, S.B. Kangc, Scripta Mater. 60 (2009) 403–406.
[28] A. Galiyev, R. Kaibyshev, T. Sakai, Mater. Sci. Forum 419–420 (2003) 509–514.
[29] S.E. Ion, F.J. Humphreys, S.H. White, Acta Metall. 30 (1982) 1909–1919.
[30] F.J. Humphreys, Recrystallization and Related Annealing Phenomena, second ed., Elsevier Ltd., Amsterdam, 2004.
[31] T. Al-Samman, G. Gottstein, Scripta Mater. 59 (2008) 760–763.
[32] L. Shanga, I.H. Junga, S. Yuea, R. Vermab, E. Essadiqic, J. Alloys Compd. 492 (2010) 173–183.
[33] G. Zlateva, Z. Martinova, Microstructure of Metals Alloys: An Atlas of Transmission Electron Microscopy Images, CRC Press, Baca Raton, 2008.
[34] Z. Zhang, M.P. Wang, N. Jiang, S.M. Li, Mater. Sci. Eng. A 527 (2010) 6467–6473.
[35] J.W. Christian, S. Mahajant, Prog. Mater. Sci. 39 (1995) 1–157.
[36] B. Sestak, Strength of Metals and Alloys, second ed., Pergamon Press, Oxford, 1979.
[37] J.S. Pan, J.M. Hong, M.P. Tian, Introduction to Materials Science, Tsinghua University Press, Beijing, 2003.
[38] J. Koike, T. Kobayashi, T. Mukai, H. Watanabe, M. Suzuki, K. Maruyama, K. Higashi, Acta Mater. 51 (2003) 2055–2065.
[39] R.Z. Valiev, O.A. Kaibyshev, S.K. Khannanov, Phys. Status Solidi A 52 (1979) 447–453.
[40] T.G. Nieh, L.M. Hsiung, J. Wadsworth, R. Kaibyshev, Acta Mater. 46 (1998) 2789–2800.
[41] T.R. McNelly, E.W. Lee, M.E. Mills, Metall. Trans. A 17 (1986) 1035–1041.